Benchmarking Torque Control Strategies for a Torsion based Series Elastic Actuator

Barkan Ugurlu, *Member, IEEE,* Emre Sariyildiz, *Member, IEEE,* Ahmet Talha Kansizoglu, Erim Can Ozcinar, *Student Member, IEEE,* and Sinan Coruk *Student Member, IEEE*

***Abstract*—This paper aims to present a comprehensive benchmarking study concerning the state-of-the-art robust torque control methods for torsion-based series elastic actuators (SEAs). Recently, several torsion-based SEAs have been proposed due to their practical advantages, e.g., high output stiffness to reduce coupling effects, spring linearity, improved yield torque, and compactness. Equipped with high-resolution encoders, these SEA units are usually built for tasks that demand high torque output. The torque controller of a SEA is mostly utilized as a low-level inner loop controller so that high-level tasks can be planned hierarchically in a decentralized control architecture. For this target architecture, the following qualities are required: i) low computational load and practicality, ii) disturbance attenuation capability. In the literature, there are experimentally verified torque controllers that can possess these properties; yet, a benchmarking study has not been performed. To this end, we defined 5 key controllers and experimentally compared their torque control performances for a comprehensive benchmarking. The experiment results obtained from a state-of-the-art torsion-based SEA unit are presented and discussed.**

***Index Terms*—series elastic actuator, torque control, benchmarking.**

I. Introduction

The diversity in torque-controlled actuators enabled researchers to address numerous pHRI (physical Human-Robot Interaction) applications with enhanced safety, dependability and interaction capability [1]. Yet, only a few of these listed torque-controlled actuators meet the challenging application requirements, i.e., mobility, improved torque/mass ratio and structural integrability. To this end, SEAs are defended to meet these requirements [2], and they are utilized in state-of-the-art robot platforms [3]–[5].

To explain briefly, an SEA unit consists of an elastic element, usually a spring, deployed between the mechanical output (load) and an electric motor [6]. Therefore, it can be classified as a two-inertia system and this fact makes its torque control problem relatively more challenging [7]. In earlier studies, classical control methods were chosen, for instance, Pratt et al. proposed a conventional PID control to achieve torque tracking. However, the torque control performance was deemed insufficient, later they additionally implemented a feed-forward term to cancel out the unmodeled dynamics [8].

B. Ugurlu, E. C. Ozcinar, S. Coruk, and A. T. Kansizoglu are with the Dept. of Mechanical Engineering, Ozyegin University, 34794 Istanbul, Turkey. (e-mail: {barkan.ugurlu}@ozyegin.edu.tr)

E. Sariyildiz is with the School of Mechanical, Materials, Mechatronics and Biomedical Engineering, University of Wollongong, NSW 25522 Wollongong, Australia. (e-mail: emre@uow.edu.au)

This work is supported by the Scientific and Technological Research Council of Turkey (TUBITAK), with the project 215E138.

In order to challenge the two-DoF (Degrees of Freedom) control problem of SEAs, Wyeth proposed a cascaded control algorithm with an inner loop velocity control and outer loop torque control to minimize the nonlinearities, e.g., backlash and stiction [9]. This method requires relatively less computational resources and thus allows higher sampling rates in real-time implementation. Internal and external disturbances can be suppressed by using fast inner velocity control. By the same token, Heike et al., studied the stability of this cascaded control method and obtained a satisfactory torque tracking performance [10].

The robust torque control of SEAs introduces another challenging dimension as there are internal and external disturbances, e.g., friction, and load side dynamics. To ensure robustness, the implementation of observer-based control methods is a common approach in the literature [11]. In [12], Oh and Kong proposed a robust control method based on a conventional PID controller with a model-based feed-forward term and a DOB (Disturbance OBserver) which was directly applied to the SEA model using the transfer function between the SEA output torque and motor torque.

In a different approach, the SMC (Sliding Mode Control) method was adopted due to its disturbance suppression ability [13], [14]. However, the chattering problem was reported as the main concern. In the literature, it is experimentally verified that the addition of a DOB leads to reduced chattering [15]. Utilizing this information, it is possible to implement a torque controller through the use of SMC and DOB and obtained fine torque tracking with reduced chattering [16], [17].

Another powerful tool for controlling SEA units is based on differential flatness (DF), which reduces the control problem to simple algebraic expressions and thus, provides computationally effective solutions [18]. Combining with a second-order DOB, Sariyildiz et al. showed that a DF-based control strategy was efficient in suppressing disturbances for the robust control of an SEA-powered joint [19] even within the presence of modeling uncertainties and unknown environmental effects.

Other highly effective control methods include adaptive control methods and optimization-based methods [20]–[22]. While they exhibit satisfactory torque-tracking performance, the algorithmic complexity and computational power requirements associated with these controllers limit their real-time implementation. In particular, the torque control loop must be simple, fast, and computationally efficient, since it serves as a servo loop in each SEA-powered robot joint when implementing a decentralized control architecture [23]. In doing so, the computational power can be saved for higher-order controllers

that are hierarchically built on top of the torque-controlled SEAs.

In light of these aspects, we investigate the effectiveness of torque controllers that can correspond to the following qualities: i) computational effectiveness, ii) robustness against disturbances, iii) practical applicability, iv) proven stability. Considering these requirements, the candidates are determined as follows: a) cascaded control [10], b) cascaded control with DOB [24], c) observer-based direct torque control [12], d) sliding mode control with DOB [14], [16], [17], e) differential flatness control with DOB [19]. We implemented a square wave reference input, sine wave reference inputs at 4 distinct frequencies, and a chirp signal reference input with a varying frequency ranging from 0.1 to 25 Hz. Torque tracking performances and Bode plots are presented for a quantifiable benchmarking.

In the literature, comparison studies were performed for modeling and design aspects of SEAs [25], [26]; however, a benchmarking study to compare the existing controllers is yet to be found to the authors' knowledge. Therefore, this paper contributes toward this direction; implementing five effective controllers on a common platform, torque control performances are presented. In section II, the benchmarked controllers are briefly explained. Results are presented and discussed in sections III and IV, respectively. Finally, the paper is concluded in section V.

II. Methods: Robust Torque Control of SEAs

In this section, we succinctly disclose the five torque controllers that are chosen for experimental benchmarking. Refer to the supplementary material for details regarding the synthesis of controllers and as well as the mathematical model of SEAs.

A. Cascaded PID Controller

The cascaded controller configuration can be seen in Fig. 1, where the superscript ref denotes the reference. θ_m, θ_s are motor angle and spring deflection, τ_m and τ_d are motor side and link side torque values, K_s is the spring stiffness. K_{p1}, K_{i1}, and K_{d1} are the proportional, integral and derivative gains of the outer loop respectively. T_d is the time constant of the motor velocity filter and ω_d is the low pass filter frequency for obtaining the rate change of torque measurement. K_{p2} and K_{i2} are the proportional and integral gains of the inner loop.In this control configuration, the outer loop has the the output torque feedback and a PID controller. The output of the PID controller generates the motor velocity reference. The PI controller achieves the velocity control at the inner loop for a given calculated velocity reference. The controller gains are tabulated in Table I. To determine the inequality constraints regarding the controller gains, refer to the stability analysis provided in [10].

B. Cascaded PID Controller with DOB

The performance of the cascaded PID controller is directly linked to the inner loop tracking performance. As the inner loop is mainly responsible for motor velocity tracking, its tracking performance can be increased with the help of a DOB that is implemented to the motor side [11], [24], [27]. The cascaded controller with a motor side DOB configuration can be seen in Fig. 2, where g is the low pass filter of the DOB, J_m is the rotor inertia, and $\hat{d}_m$ is the estimated motor side disturbance. The tuning of the controller follows the same rules as in the previous method. The controller gains are listed in Table II.

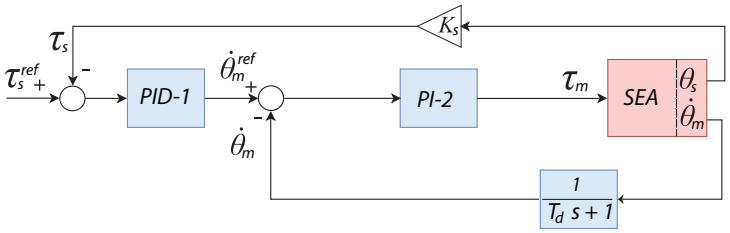

Fig. 1. Block diagram of the Cascaded PID Control with an inner velocity loop.

TABLE I
Cascaded PID Controller parameters

Parameter	*Value*
Outer loop proportional gain (K_{p1})	16
Outer loop integral gain (K_{i1})	7
Outer loop derivative gain (K_{d1})	0.8
Cut-off frequency in PID (w_d)	1600 Hz
Inner loop proportional gain (K_{p2})	0.045
Inner loop integral gain (K_{i2})	0.012
Motor velocity filter time constant (T_d)	1/600 s

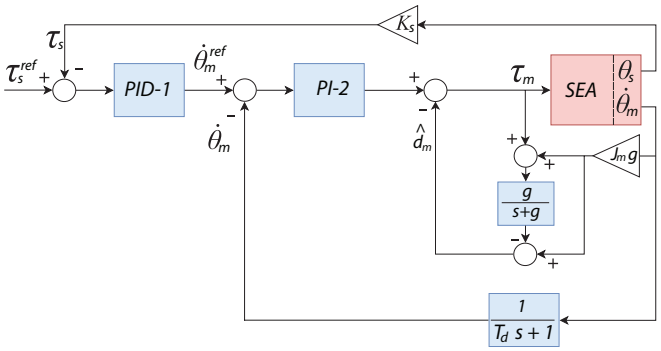

Fig. 2. Block diagram of the Cascaded PID Control with inner velocity loop and DoB.

TABLE II
Cascaded PID Controller+DOB parameters.

Parameter	*Value*
Outer loop proportional gain (K_{p1})	3.5
Outer loop integral gain (K_{i1})	0.6
Outer loop derivative gain (K_{d1})	0.023
Cut-off frequency of PID (w_d)	1600 Hz
Inner loop proportional gain (K_{p2})	0.15
Inner loop integral gain (K_{i2})	0.05
Motor velocity filter time constant (T_d)	1/600 s
Low pass frequency of DOB (g)	600 Hz

C. PID with model based feed-forward and DOB

In contrast to the previous method in which DOB is configured solely at the motor side, one alternative way is based on considering the overall SEA transfer function defined between the link torque output and motor torque input. With the addition of feed-forward and feedback terms to this DOB block, Oh and Kong proposed a robust model-based control algorithm in [12]. High precision tracking is addressed by means of spring deflection feedback. The controller scheme can be seen in Fig. 3.

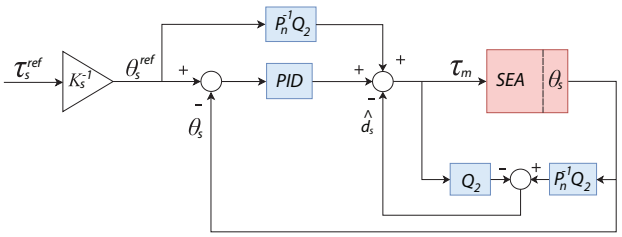

Fig. 3. Block diagram of the PID with model based feed-forward and DoB

TABLE III
FF+PID+DOB PARAMETERS

Parameters	*Value*
Proportional gain (K_p)	100
Integral gain (K_i)	100
Derivative gain (K_d)	14
Cut-off frequency in PID (w_d)	300 Hz
Cut-off frequency of Q_2 (w_c)	1600 Hz
Cut-off frequency of Q_1 (w_v)	628 Hz

In this figure, P_n is the nominal model. $\hat{d}_s$ is the estimated disturbance acting on the spring; see the supplementary file for further details. Q_2 is a second order low-pass Butterworth filter with a cut-off frequency of ω_c:

$$Q_2(s) = \frac{\omega_c^2}{s^2 + \sqrt{2}\omega_c s + \omega_c^2} \tag{1}$$

Both the feed-forward term and the DOB contain the inverse of the nominal model. To realize P_n^{-1}, a second-order Butterworth filter with a cut-off frequency ω_c is used [28]. The feedback term is the PID controller that is tuned with respect to the nominal plant. The controller gains are provided in Table III. Refer to [12] for further details.

D. Sliding mode control with DOB

A sliding mode controller is known to be highly suitable for controlling the systems that suffer from modeling uncertainties and disturbances [13]. Fundamentally, an SMC defines a sliding surface that is constructed by using system states, and the aim of the controller is defined as confining the sliding variable to a certain close neighborhood [29].

Depending on the sign of the sliding variable, the control action switches between different values within a discrete signal profile. The switching action sensitivity and the decay rate of the sliding trajectory can be determined by controller parameters by considering a well-known problem: chattering [14], [15]. To that end, we utilized the approach proposed in [16] where a sliding mode controller with a disturbance observer was synthesized to overcome the chattering phenomenon; see Fig. 4. The controller gains are provided in IV. Refer to the supplementary file for the synthesis of this controller.

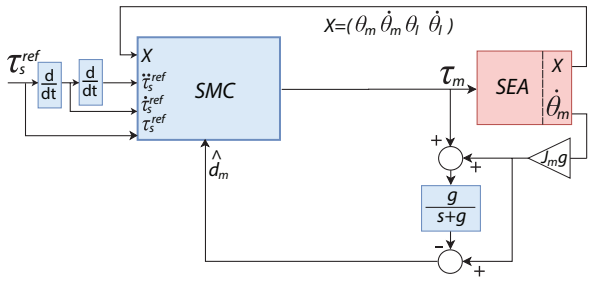

Fig. 4. Block diagram of the Sliding Mode Controller with DOB.

TABLE IV
SMC+DOB PARAMETERS

Parameters	*Value*
Convergence rate (c)	500
SMC gain (ρ)	1.6
Cut-off frequency, motor velocity (w_{θ_m})	1000 Hz
Cut-off frequency, deflection rate change (w_{θ_s})	1000 Hz
Low pass frequency of DOB (g)	1500 Hz

E. Differential Flatness Control with DOB

Differential flatness control was proposed by Fliess et al. mainly for motion planning applications of the systems that are differentially flat. A system is called differentially flat if all system states, inputs and outputs are expressible with the different combinations of flat output variables and its derivatives that are not differentially coupled [30]. While useful in handling nonlinearities, differential flatness control itself may not possess the robustness property as it is usually sensitive to uncertainties [19]. In order to benefit the useful properties of differential flatness while handling uncertainties, Sariyildiz and Yu proposed a high-order disturbance observer in state space and combined it with a DF-based controller design [19]; see Fig. 5. In this figure k symbolizes the diagonal state-space feedback gain matrix. We adopted this strategy and implemented a torque controller whose gains are given in Table V. Refer to the supplementary material for the synthesis of this controller.

TABLE V
DF+DOB PARAMETERS.

Parameters	*Value*
Proportional gain (K_p)	1.1
Derivative gain (K_d)	0.21
Cut-off frequency of PID (w_d)	150 Hz
Cut-off frequency of DOB (g)	300 Hz

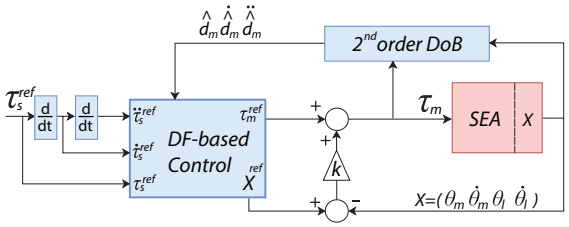

Fig. 5. Block diagram of the DF+DoB controller. To estimate the disturbances d_1 and d_2 and their derivatives, a second order DOB was implemented; see [19].

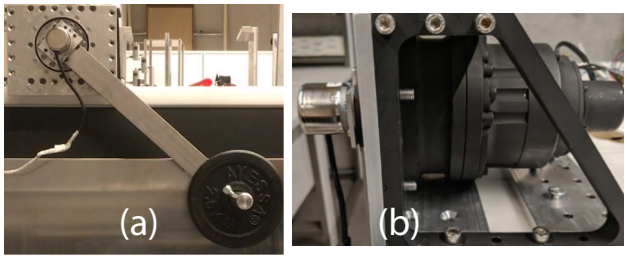

Fig. 6. A state-of-the-art SEA unit was used as the experiment testbed. a) From the front side, b) from sideways.

III. Results

A. Hardware Testbed

In order to experimentally compare the listed controllers, we conducted a series of experiments using a state-of-the-art SEA unit built *in-house* [31]; see Fig. 6. It was constructed using a frameless-brushless motor (Kollmorgen TBM-7631) whose mechanical output was coupled with a Harmonic Drive gear (CSG-25, 1:100). A custom-built torsional spring with a stiffness of 91 Nm/deg was placed between the SEA output and the Harmonic Drive gear. Two 23-bit resolution encoders (Broadcom AS38-H39E-S13S) were deployed to measure deflection and motor side angle separately. The mechanical output of the SEA was connected to a 0.4 m long link that weighs at 1.2 kg. A dummy load of 2.5 kg was attached at the tip of the link.

Electronics hardware implementation of the experimental setup included a custom-built PCB for reading the encoders and interfacing with the motor driver via digital-to-analog converters. As the motor drive, an ESCON 70/10 was used. The main controller was an ARM-based PC running on a real-time Linux with a sampling frequency of 2 kHz. Discrete domain transformations of the continuous models were obtained via bilinear transformation.

In order to yield a thorough experimental analysis, each controller was tested using the following inputs: i) square wave, ii) sine wave, iii) chirp signal. In each case, we empirically tuned the controller gains in accordance with the standard rules of linear controller design; stability and non-excitation of unmodeled nonlinear dynamics. These gains are populated for each controller in Tables I-V.

B. Simulations : Frequency Sweep

Prior to the experimental study, all five controllers were simulated using the Compliant Joint Toolbox (CJT) [32]. To this end, a realistic model of our testbed was constructed in CJT and the controllers were synthesized accordingly. Applying a chirp signal with a frequency ranged from 0.1 Hz to 25 Hz, magnitude and phase response of each controller was obtained in the frequency domain. Therefore, we were able to display the bandwidth of each controller. Fig. 7 shows the Bode diagram of each controller where we indicated the intersection of -3 dB with a small box.

The bandwidths of Cascaded PID, Cascaded PID+DOB, FF+PID+DOB, SMC+DOB, and DF+DOB are 18.6 Hz, 18.6 Hz, 19 Hz, 23.6 Hz, and 18.9 Hz, respectively. Observing this result, we may judge that all five controllers performed relatively well. Nevertheless, SMC+DOB distinguishes itself from the rest as it has the the largest control bandwidth.

C. Experiments: Square Wave Reference Tracking

A square wave signal with a peak-to-peak amplitude of 20 Nm and a frequency of 0.25 Hz was implemented. This reference signal also indicates the step response of each controller. Results can be seen in Fig. 8, first column, in which solid red and dashed blue lines respectively indicate measured torque and reference input. The first two overshoots were also zoomed-in and displayed for each plot for a clear examination. Table VI lists the maximum overshoot percentage (M_p), settling time (t_s), and RMS (Root Mean Square) of tracking error (e_{RMS}).

TABLE VI
The Controller Performances for the Square Wave Input.

Controller Name	M_p	t_s (s)	e_{RMS} (Nm)
Cascaded PID	23%	0.3	1.33
Cascaded PID+DOB	27%	0.16	1.27
FF+PID+DOB	3%	0.21	1.36
SMC+DOB	5%	0.15	1.44
DF+DOB	23%	0.3	1.59

Examining these results, we can validate that all the controller provided acceptable tracking performances. The variation of e_{RMS} values is considerably low ($M = 1.4$, $SD = 0.12$), suggesting that torque tracking is achieved for all 5 cases. On the contrary, we observe a clear variation in M_p values, in which FF+PID+DOB and SMC+DOB outperform other controllers. From the setting time perspective, Cascaded PID+DOB and SMC+DOB suggest relatively more favorable results as they settled within 0.16 s.

D. Experiments: Sinusoidal Reference Tracking

Sinusoidal wave signals with a peak-to-peak amplitude of 20 Nm were implemented at 4 distinct frequencies: 0.48 Hz, 0.96 Hz, 1.91 Hz, and 4.4 Hz. Results can be seen in Fig. 8, second column, and in Fig. 8, third column, where solid red and dashed blue lines respectively stand for measured torque and reference input. Furthermore, Table VII lists e_{RMS} values

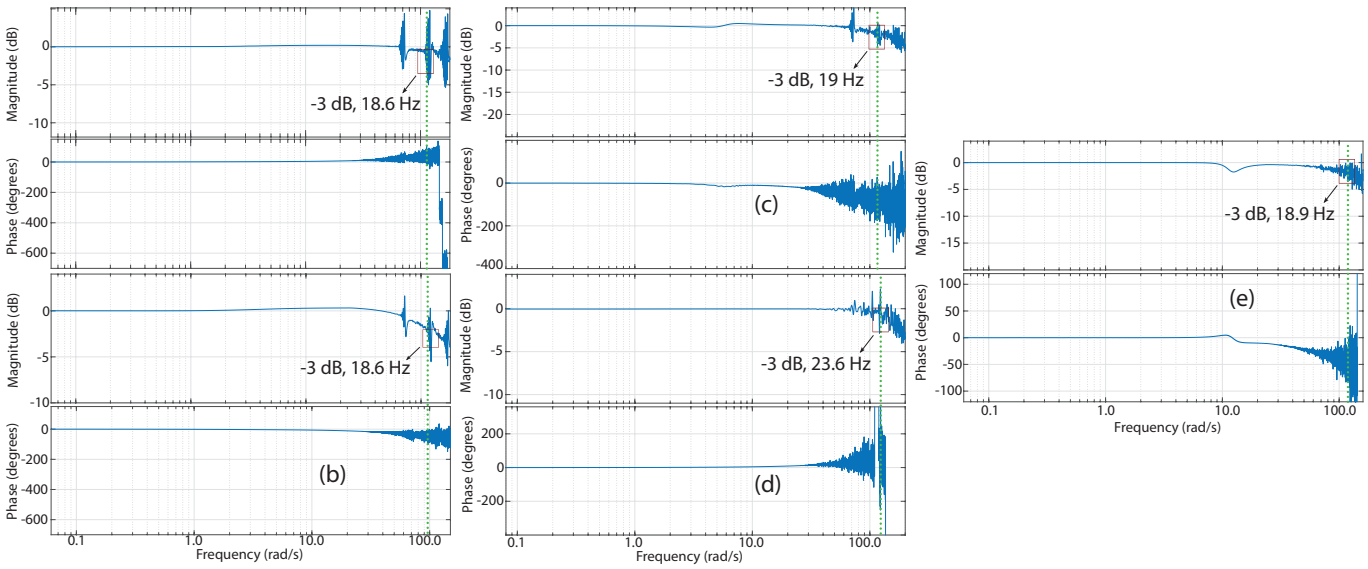

Fig. 7. The bandwidth of each controller is obtained via frequency sweeping from 0.1 Hz to 25 Hz: a) Cascaded PID, b) Cascaded PID+DOB, c) FF+PID+DOB, d) SMC+DOB, e)DF+DOB.

TABLE VII
SINE WAVE TRACKING PERFORMANCES: e_{RMS} VALUES.

Controller	*0.48 Hz*	*0.96 Hz*	*1.91 Hz*	*Chirp*
Cascaded PID	0.283	0.313	0.366	0.452
Cascaded PID+DOB	0.228	0.329	0.501	0.804
FF+PID+DOB	0.347	0.682	1.309	1.060
SMC+DOB	0.208	0.251	0.361	0.445
DF+DOB	0.233	0.507	1.133	0.849

for 4 cases: a) 0.48 Hz, 0.96 Hz, 1.91 Hz, and a chirp signal with a varying frequency of 0.0-5.0 Hz.

These results suggest that all the controllers perform well for lower frequency input; however, the tracking performance deteriorates as the frequency increases, particularly for the case of FF+PID+DOB. Assessing all sine wave tracking results, SMC+DOB appears to outperform the other controllers as it provided high fidelity tracking.

E. Experiments: Frequency Sweep

Implementing a chirp signal with a frequency ranged from 0.1 Hz to 25 Hz, magnitude and phase response of each controller was obtained in the frequency domain. In doing so, we were able to display the bandwidth of each controller. Fig. 9 displays the Bode diagram of each controller, in which the intersection of -3 dB was indicated with a small box.

The bandwidths of Cascaded PID, Cascaded PID+DOB, FF+PID+DOB, SMC+DOB, and DF+DOB are 17 Hz, 16.7 Hz, 11 Hz, 19 Hz, and 13 Hz, respectively. SMC+DOB has the largest controller bandwidth and this comes with no surprise as it provided best torque tracking performance in previous experiments as well. This results is also in harmony with the simulation results depicted in Fig. 7. The main difference is that FF+PID+DOB and DF+DOB performed relatively better in simulation, compared to experiments. This may indicate potential real-life applicability issues concerning these controllers.

IV. DISCUSSION

In light of the experiment results, we can conclude that SMC+DOB appears to be more favorable when compared to other controllers in terms of torque tracking. Considering the fact that SEA modeling is prone to parametric uncertainties and modeling errors, the SMC-based controller performs well as it has the intrinsic capability of disturbance attenuation [33]. Combining it with a DOB surely enhances its performance [15], as the sole implementation of SMC suffers from chattering and this phenomenon is much more apparent for a two-inertia systems like SEAs.

It is evident that DOB, in general, performs well for the torque control problem of series elastic actuators. It eliminated disturbances due to modeling uncertainties and controller structure, e.g., chattering. A similar result was also reported for an SEA unit with a highly soft spring (0.48 Nm/rad) [12]. In light of these facts, the DOB appears to be an integral part of a torque controller to achieve fine tracking. At this point, we highlight the fact that the inner loop bandwidth is one of the dominant factors in the passive rendering of virtual impedance without violating the stability [34].

In order to eliminate coupling effects between joint stiffness and robot dynamics, we deliberately designed a stiff spring [31] and this approach is prevalent for robots with decentralized torque controllers [23]. While the benefits of using a stiff spring are of critical importance, deflection measurements suffer from noise and torque resolution. Using high resolution (23-bits) encoders may eliminate the latter; yet, measurement noise appears to be of critical importance. As a matter of this fact, differentiating noisy sensory data forced us to use filters with relatively lower cut-off frequencies which could limit the controller bandwidth.

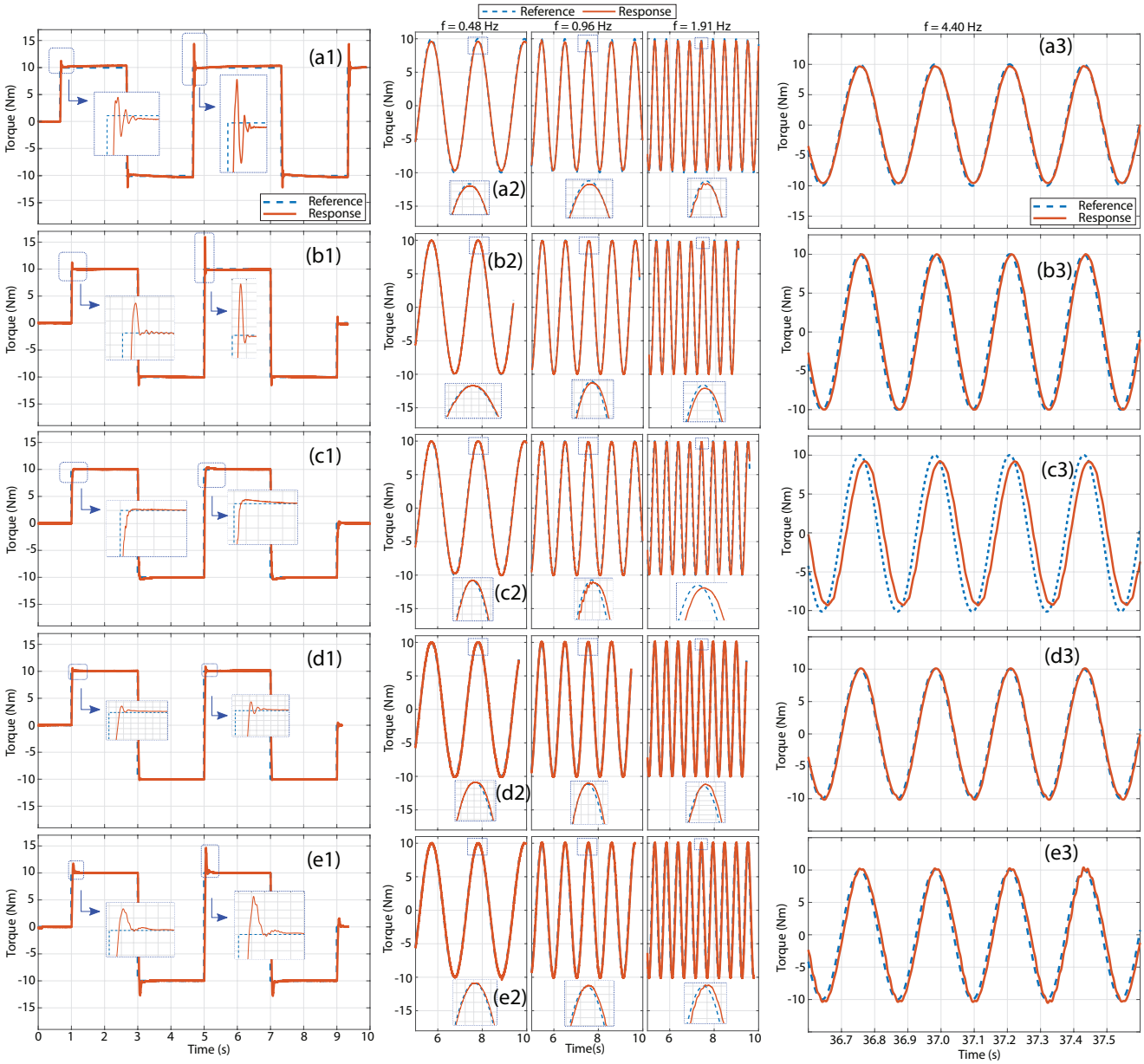

Fig. 8. Tracking performances. 1^{st} column: square wave inputs, 2^{nd} column: sine wave inputs with frequencies of 0.48 Hz, 0.96 Hz, and 1.91 Hz, 3^{rd} column: sine wave inputs with a frequency of 4.4 Hz. (a) row: cascaded PID, (b) row: cascaded PID+DOB, (c) row: FF+PID+DOB, (d) row: SMC+DOB, (e) row: DF+DOB.

In a recent simulation study, we observed that MPC (Model Predictive Control) exhibits superior performance concerning the torque tracking problem of SEAs [22]. This finding may be generalized in a sense that optimization-based methods are deemed to be powerful tools for this matter [20], [21]. On the contrary, the computational cost and algorithmic complexity associated with these controllers limit their real-time implementation for the decentralized control approach [23]. Therefore, the benchmarking study in this paper is limited with controllers which can be reliably implemented in real-time without the violation of constant sampling rate at 2 kHz.

In this work, all the controller gains are empirically tuned in accordance with the standard rules of linear controller design; stability and non-excitation of unmodeled nonlinear dynamics. Although we devoted the utmost care to obtain the best possible performance in each case, a possible sub-optimal gain tuning may be a limitation in this work. That being said, SMC+DOB and DF+DOB possess a clear advantage in this case as they only have two controller gains to be tuned. While the incorporation of an adaptive gain tuning algorithm may eliminate this problem, it may increase the computational complexity and therefore may not be a suitable choice for an inner loop torque-controller as stated previously.

V. Conclusion

In this work, we presented an experimental benchmarking study of 5 distinct controllers which are computationally-effective and can exhibit sufficient torque tracking perfor-

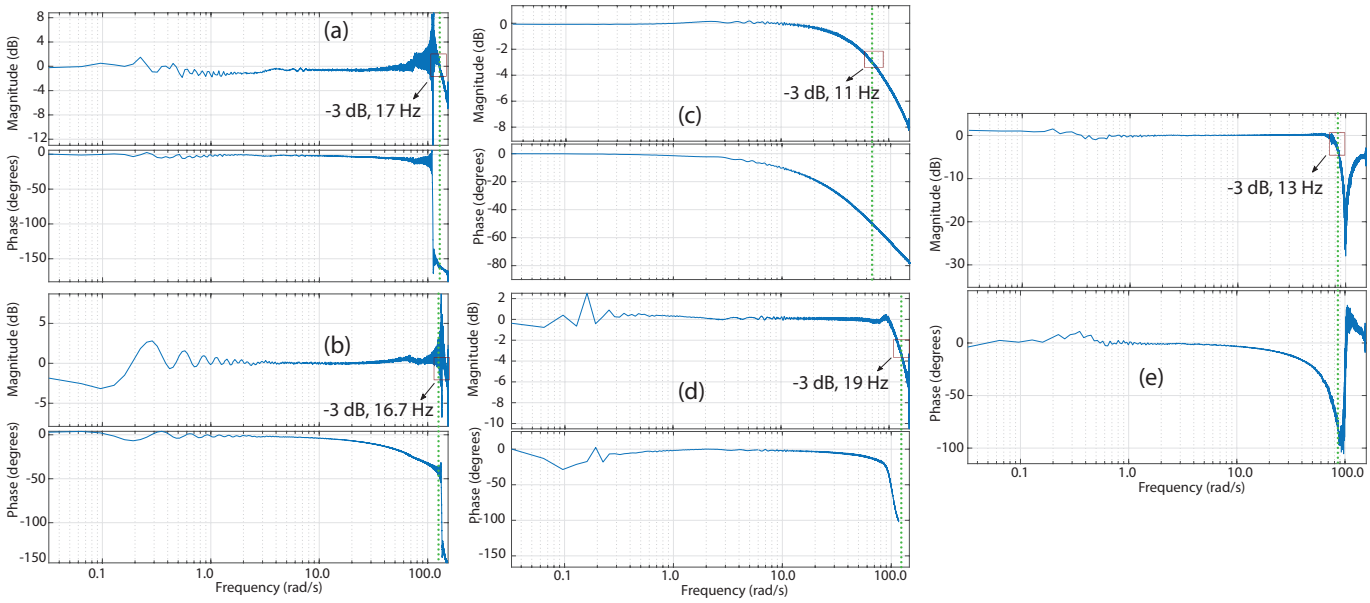

Fig. 9. The bandwidth of each controller is obtained via frequency sweeping from 0.1 Hz to 25 Hz: a) Cascaded PID, b) Cascaded PID+DOB, c) FF+PID+DOB, d) SMC+DOB, e)DF+DOB.

mance for a torsion-based SEA unit. Supported with a disturbance observer, they are deemed to provide satisfactory results as they can assume the role of low-level controller for a decentralized robot control approach [23]. Among these controllers, SMC+DOB appeared to have more favorable performance and its control bandwidth was the largest: 19 Hz.

The use of series elastic actuators is widespread in the robotics community, particularly for the torque-controlled systems. In this sense, the current work also provided a succinct guideline for the practical implementation of these torque controllers. One may choose one of these controllers depending on the task and the range of frequency for the particular application.

REFERENCES

[1] R. Ham, T. Sugar, B. Vanderborght, K. Hollander, and D. Lefeber, "Compliant actuator designs," *IEEE Robotics & Automation Magazine*, vol. 16, no. 3, pp. 81–94, Sep. 2009.

[2] H. Vallery, J. Veneman, E. van Asseldonk, R. Ekkelenkamp, M. Buss, and H. van Der Kooij, "Compliant actuation of rehabilitation robots," *IEEE Robotics & Automation Magazine*, vol. 15, no. 3, pp. 60–69, Sep. 2008.

[3] N. Paine, J. S. Mehling, J. Holley, N. A. Radford, G. Johnson, C.-L. Fok, and L. Sentis, "Actuator control for the NASA-JSC valkyrie humanoid robot: A decoupled dynamics approach for torque control of series elastic robots," *Journal of Field Robotics*, vol. 32, no. 3, pp. 378–396, Jan. 2015.

[4] S. Wang, L. Wang, C. Meijneke, E. van Asseldonk, T. Hoellinger, G. Cheron, Y. Ivanenko, V. L. Scaleia, F. Sylos-Labini, M. Molinari, F. Tamburella, I. Pisotta, F. Thorsteinsson, M. Ilzkovitz, J. Gancet, Y. Nevatia, R. Hauffe, F. Zanow, and H. van der Kooij, "Design and control of the MINDWALKER exoskeleton," *IEEE Transactions on Neural Systems and Rehabilitation Engineering*, vol. 23, no. 2, pp. 277–286, Mar. 2015.

[5] J. Veneman, R. Kruidhof, E. Hekman, R. Ekkelenkamp, E. V. Asseldonk, and H. van der Kooij, "Design and evaluation of the LOPES exoskeleton robot for interactive gait rehabilitation," *IEEE Transactions on Neural Systems and Rehabilitation Engineering*, vol. 15, no. 3, pp. 379–386, Sep. 2007.

[6] G. A. Pratt, M. M. Williamson, P. Dillworth, J. Pratt, and A. Wright, "Stiffness isn't everything," in *Experimental Robotics IV*. Springer-Verlag, pp. 253–262.

[7] Y. Yokokura and K. Ohishi, "Fine load-side acceleration control based on torsion torque sensing of two-inertia system," *IEEE Transactions on Industrial Electronics*, vol. 67, no. 1, pp. 768–777, Jan. 2020.

[8] G. Pratt, P. Willisson, C. Bolton, and A. Hofman, "Late motor processing in low-impedance robots: impedance control of series-elastic actuators," in *Proceedings of the 2004 American Control Conference*. IEEE, 2004.

[9] G. Wyeth, "Control issues for velocity sourced series elastic actuators," in *Proceedings of the Australian Conf. Robot. Autom.*, 2006.

[10] H. Vallery, R. Ekkelenkamp, H. van der Kooij, and M. Buss, "Passive and accurate torque control of series elastic actuators," in *2007 IEEE/RSJ International Conference on Intelligent Robots and Systems*. IEEE, Oct. 2007.

[11] K. Kong, J. Bae, and M. Tomizuka, "Control of rotary series elastic actuator for ideal force-mode actuation in human–robot interaction applications," *IEEE/ASME Transactions on Mechatronics*, vol. 14, no. 1, pp. 105–118, Feb. 2009.

[12] S. Oh and K. Kong, "High-precision robust force control of a series elastic actuator," *IEEE/ASME Transactions on Mechatronics*, vol. 22, no. 1, pp. 71–80, Feb. 2017.

[13] J. Bae, K. Kong, and M. Tomizuka, "Gait phase-based smoothed sliding mode control for a rotary series elastic actuator installed on the knee joint," in *Proceedings of the 2010 American Control Conference*. IEEE, Jun. 2010.

[14] A. Calanca, L. Capisani, and P. Fiorini, "Robust force control of series elastic actuators," *Actuators*, vol. 3, no. 3, pp. 182–204, Jul. 2014.

[15] A. Kawamura, H. Itoh, and K. Sakamoto, "Chattering reduction of disturbance observer based sliding mode control," *IEEE Transactions on Industry Applications*, vol. 30, no. 2, pp. 456–461, 1994.

[16] E. Sariyildiz, R. Mutlu, and H. Yu, "A sliding mode force and position controller synthesis for series elastic actuators," *Robotica*, vol. 38, no. 1, pp. 15–28, Apr. 2019.

[17] M. Wang, L. Sun, W. Yin, S. Dong, and J. Liu, "A novel sliding mode control for series elastic actuator torque tracking with an extended disturbance observer," in *2015 IEEE International Conference on Robotics and Biomimetics (ROBIO)*. IEEE, Dec. 2015.

[18] M. Fliess, J. Lévine, P. Martin, and P. Rouchon, "On differentially flat nonlinear systems," *IFAC Proceedings Volumes*, vol. 25, no. 13, pp. 159–163, Jun. 1992.

[19] E. Sariyildiz and H. Yu, "A robust force controller design for series elastic actuators," in *2017 IEEE/RSJ International Conference on Intelligent Robots and Systems (IROS)*. IEEE, Sep. 2017.

[20] A. Calanca and P. Fiorini, "Human-adaptive control of series elastic actuators," *Robotica*, vol. 32, no. 8, pp. 1301–1316, Jul. 2014.

[21] J. C. Perez-Ibarra, A. L. J. Alarcon, J. C. Jaimes, F. M. E. Ortega, M. H. Terra, and A. A. Siqueira, "Design and analysis of $h\infty$ force control of a series elastic actuator for impedance control of an ankle rehabilitation robotic platform," in *2017 American Control Conference (ACC)*. IEEE, May 2017.

[22] A. T. Kansizoglu, E. Sariyildiz, and B. Ugurlu, "A comparison study on observer-based force control of series elastic actuators," in *2018 IEEE 15th International Workshop on Advanced Motion Control (AMC)*. IEEE, Mar. 2018.

[23] N. Paine, J. S. Mehling, J. Holley, N. A. Radford, G. Johnson, C.-L. Fok, and L. Sentis, "Actuator control for the NASA-JSC valkyrie humanoid robot: A decoupled dynamics approach for torque control of series elastic robots," *Journal of Field Robotics*, vol. 32, no. 3, pp. 378–396, Jan. 2015.

[24] W. Roozing, J. Malzahn, D. G. Caldwell, and N. G. Tsagarakis, "Comparison of open-loop and closed-loop disturbance observers for series elastic actuators," in *2016 IEEE/RSJ International Conference on Intelligent Robots and Systems (IROS)*. IEEE, Oct. 2016.

[25] C. Lee, S. Kwak, J. Kwak, and S. Oh, "Generalization of series elastic actuator configurations and dynamic behavior comparison," *Actuators*, vol. 6, no. 3, p. 26, Aug. 2017.

[26] J. Hurst, A. Rizzi, and D. Hobbelen, "Series elastic actuation: Potential and pitfalls," in *Int. Conf. on Climbing and Walking Robots*. Springer, Mar. 2004.

[27] K. Ohnishi, M. Shibata, and T. Murakami, "Motion control for advanced mechatronics," *IEEE/ASME Transactions on Mechatronics*, vol. 1, no. 1, pp. 56–67, Mar. 1996.

[28] J. S. Mehling, J. Holley, and M. K. O'Malley, "Leveraging disturbance observer based torque control for improved impedance rendering with series elastic actuators," in *2015 IEEE/RSJ International Conference on Intelligent Robots and Systems (IROS)*. IEEE, Sep. 2015.

[29] V. Utkin, "Sliding mode control design principles and applications to electric drives," *IEEE Transactions on Industrial Electronics*, vol. 40, no. 1, pp. 23–36, Feb. 1993.

[30] M. Fliess, J. Lévine, P. Martin, and P. Rouchon, "Differential flatness and defect: an overview," *Banach Center Publications*, vol. 32, no. 1, pp. 209–225, 1995.

[31] M. C. Yildirim, P. Sendur, O. Bilgin, B. Gulek, G. G. Yapici, and B. Ugurlu, "An integrated design approach for a series elastic actuator: Stiffness formulation, fatigue analysis, thermal management," in *2017 IEEE-RAS 17th International Conference on Humanoid Robotics (Humanoids)*. IEEE, Nov. 2017.

[32] J. Malzahn, W. Roozing, and N. Tsagarakis, "The compliant joint toolbox for matlab: An introduction with examples," *IEEE Robotics & Automation Magazine*, vol. 26, no. 3, pp. 52–63, Sep. 2019.

[33] J. M. A.-D. Silva, C. Edwards, and S. K. Spurgeon, "Sliding-mode output-feedback control based on LMIs for plants with mismatched uncertainties," *IEEE Transactions on Industrial Electronics*, vol. 56, no. 9, pp. 3675–3683, Sep. 2009.

[34] T. Boaventura, G. A. Medrano-Cerda, C. Semini, J. Buchli, and D. G. Caldwell, "Stability and performance of the compliance controller of the quadruped robot HyQ," in *2013 IEEE/RSJ International Conference on Intelligent Robots and Systems*. IEEE, Nov. 2013.